The androgen receptor in mesenchymal progenitors regulates skeletal muscle mass via *Igf1* expression in male mice

Hiroshi Sakai[1,2,*], Hideaki Uno[2], Harumi Yamakawa[2], Kaori Tanaka[3], Aoi Ikedo[1], Akiyoshi Uezumi[4], Yasuyuki Ohkawa[3], Yuuki Imai[1,2,*]

[1]Division of Integrative Pathophysiology, Proteo-Science Center, Ehime University, Toon, Ehime 791-0295, Japan.

[2]Department of Pathophysiology, Ehime University Graduate School of Medicine, Toon, Ehime 791-0295, Japan.

[3]Division of Transcriptomics, Medical Institute of Bioregulation, Kyushu University, Higashi-ku, Fukuoka 812-0054, Japan.

[4]Divison of Cell Heterogeneity, Medical Institute of Bioregulation, Kyushu University, Higashi-ku, Fukuoka 812-0054, Japan.

[*]Hiroshi Sakai, Yuuki Imai

Email: sakai.hiroshi.wh@ehime-u.ac.jp (H.S.), y-imai@m.ehime-u.ac.jp (Y.I.)

Hiroshi Sakai, DVM, PhD, or Yuuki Imai, MD, PhD, Proteo-Science Center, Graduate School of Medicine, Ehime University, Shitsukawa, Toon, Ehime, 791-0295, Japan.

Author Contributions: Conceptualization, H.S. and Y.I.; Methodology, H.S., H.U., K.T., A.I., A.U., Y.O., and Y.I.; Software, H.S., H.U., and K.T.,; Investigation, H.S., H.U., H.Y., K.T., and A.I.; Writing – Original Draft, H.S., and Y.I.; Writing – Review & Editing, H.S., and Y.I.;

Funding Acquisition, H.S., and Y.I.; Resources, H.S., K.T., A.U., Y.O., and Y.I.; Supervision, H.S., and Y.I.

Competing Interest Statement: The authors declare no competing interests.

Classification: Biological Sciences, Medical Sciences

Keywords: androgen receptor, skeletal muscle, mesenchymal progenitors, Igf1

Funding: This work was supported in part by MEXT/JSPS KAKENHI (JP21K17568 to H.S.; JP22H03203 to Y.I.) and the HIRAKU-Global Program, which is funded by MEXT's "Strategic Professional Development Program for Young Researchers" and Takeda Science Foundation (to H.S.).

Abstract

Androgens exert their effects primarily by binding to the androgen receptor (AR), a ligand-dependent nuclear receptor. While androgens have anabolic effects on skeletal muscle, previous studies reported that AR functions in myofibers to regulate skeletal muscle quality, rather than skeletal muscle mass. Therefore, the anabolic effects of androgens are exerted via extra-myofiber cells or tissues. In this context, the cellular and molecular mechanisms of AR in mesenchymal progenitors, which play a crucial role in maintaining skeletal muscle homeostasis, remain largely unknown. In this study, we demonstrated expression of AR in mesenchymal progenitors and found that targeted AR ablation in mesenchymal progenitors reduced limb muscle mass in mature adult, but not young or aged, male mice, although fatty infiltration of muscle was not affected. The absence of AR in mesenchymal progenitors led to remarkable perineal muscle hypotrophy, regardless of age, due to abnormal regulation of transcripts associated with apoptosis and extracellular matrix organization. Additionally, we revealed that AR in mesenchymal progenitors regulates the expression of insulin-like growth factor 1, which can increase skeletal muscle mass in a paracrine manner. These findings indicate that the anabolic effects of androgens regulate skeletal muscle mass via, at least in part, AR signaling in mesenchymal progenitors.

54 **Significance statement**

55 Androgens are essential not only for the development of male sexual characteristics but also for a
56 range of physiological functions, including the regulation of skeletal muscle growth and
57 function. Understanding the functionality of the androgen receptor (AR) is essential for
58 comprehending the mechanisms through which androgens exert their effects on skeletal muscles,
59 as these effects are mediated through AR binding. Our study demonstrates that AR is expressed
60 in mesenchymal progenitors, which play a vital role in muscle homeostasis, and regulates the
61 expression of insulin-like growth factor 1 (Igf1)—a key player in skeletal muscle growth—to
62 control muscle mass. Combining androgens and IGF1 treatments may offer potential therapeutic
63 approaches for addressing muscle atrophy conditions such as sarcopenia.

64 **Introduction**

65 Androgens are crucial regulators of various biological processes, including the development and
66 maintenance of male characteristics. Notably, in a physiological context, the administration of
67 androgens or androgen analogs has been shown to exert anabolic effects on muscles, resulting in
68 increased muscle mass, strength, and body weight (1, 2). These physiological effects are
69 mediated by activation of the androgen receptor (AR), a member of the nuclear receptor
70 superfamily (3). However, despite that clinical administration of androgens in men can
71 successfully increase skeletal muscle mass (4), the precise cellular and molecular mechanisms
72 underlying the function of AR in muscle remain largely unexplored.

73 Skeletal muscle represents a complex tissue comprising multiple cell types, and the
74 effects of androgens are likely mediated by various cell populations expressing AR within
75 skeletal muscles. While male mice systemically lacking AR exhibit low skeletal muscle strength
76 and mass, similar to female levels (5), we previously showed that muscle hypertrophy can be
77 induced by androgen administration even in the absence of AR in muscle fibers, suggesting that
78 non-myofiber AR contributes to the regulation of muscle mass (6). Furthermore, another of our
79 studies demonstrated that deletion of AR in satellite cells, which are muscle stem cells
80 responsible for muscle regeneration, had a limited effect on their proliferation and differentiation
81 (7). Additionally, since limb muscle mass remains unaffected even in mice with AR ablation in
82 both myofibers and muscle stem cells (8), other cells expressing AR within the muscles may play
83 a role in regulating skeletal muscle mass.

84 Mesenchymal progenitors (9), also known as fibro/adipogenic progenitors (10), have
85 been identified as a cell population distinct from myogenic cells characterized by the expression
86 of platelet-derived growth factor receptor alpha (PDGFRα). These cells are involved in the

87 maintenance and regeneration of skeletal muscle (11, 12). Conversely, mesenchymal progenitors
88 have been implicated in pathological fibrosis and fat accumulation in skeletal muscle (13). AR
89 expression has been reported in cells located in the interstitium or outside the basal lamina in
90 both mouse and human skeletal muscles (14, 15). Additionally, ablation of AR specifically in
91 embryonic cells of the mesenchyme led to impaired development of the perineal levator ani (LA)
92 and bulbocavernosus (BC) muscles (16), which are particularly responsive to androgen.
93 Furthermore, the reduced proliferation of undifferentiated myoblasts in these mutant mice
94 suggested a potential paracrine regulatory role of mesenchymal AR in controlling skeletal
95 muscles (16). Despite this knowledge, the specific role of AR in adult mesenchymal progenitors
96 in skeletal muscles remains unexplored.
97 Here we investigate the role of AR expressed in mesenchymal progenitors in muscle
98 maintenance using mice with mesenchymal progenitor-specific AR ablation. We show that AR
99 in mesenchymal progenitors plays a critical role in maintaining skeletal muscle mass via
100 regulation of insulin-like growth factor 1 (Igf1) expression in male mice.

101 **Results**

102 **AR ablation in mesenchymal progenitors was validated in *PDGFRα-CreER;AR$^{L2/Y}$* mice**

103 AR expression in fibroblasts of the perineal LA muscles and in mesenchymal cells of the fetal
104 LA muscles has been reported (14, 16, 17); however, it is unknown whether mesenchymal
105 progenitors in adult limb muscle express AR. To examine the expression pattern of AR in
106 mesenchymal progenitors, immunofluorescence staining of PDGFRα, a marker of mesenchymal
107 progenitors (9), and AR was performed in adult (12 weeks old) male mice. We found that AR
108 was expressed in mesenchymal progenitors staining positive for PDGFRα (Fig. 1A), as well as in
109 muscle fibers surrounded by laminin-expressing basal lamina, consistent with previous findings
110 (17, 18).

111 To investigate the role of AR in mesenchymal progenitors, *PDGFRα-CreER* (19) and
112 *AR$^{L2/Y}$* (20) mice were crossed to selectively delete the AR gene in mesenchymal progenitors
113 expressing PDGFRα. Tamoxifen (TMX) was administered to Cre control male mice (*PDGFRα-*
114 *CreER*) and mutant male mice (*PDGFRα-CreER;AR$^{L2/Y}$*) for 5 consecutive days to induce AR
115 ablation (Fig. 1B). To assess the efficiency of AR ablation, immunofluorescence staining of
116 PDGFRα and AR was performed in Cre control and mutant mice. Quantification of PDGFRα
117 and AR expression in forelimb biceps brachii (BB) and hindlimb tibialis anterior (TA) muscles
118 demonstrated a significant decrease of 90% in AR protein in mutant mice compared with Cre
119 control mice, confirming successful ablation of AR expression in mesenchymal progenitors from
120 *PDGFRα-CreER;AR$^{L2/Y}$* mice (Fig. 1C). Taken together, these findings demonstrate successful
121 and specific loss of AR expression in PDGFRα+ cells, rendering them an optimal model for
122 investigating AR in mesenchymal progenitors in skeletal muscles.

123

124 **Lack of AR in mesenchymal progenitors had a limited effect on steady-state limb skeletal**
125 **muscles**
126 Because ablation of PDGFRα+ cells in intact muscles results in skeletal muscle atrophy (11, 12),
127 we first analyzed the muscles of Cre control and mutant mice under steady-state conditions at a
128 young age (14 weeks old) (Fig. S1A). Body weight and limb skeletal muscle mass were not
129 affected in mutant compared with control mice at 2 weeks after TMX administration (Fig. S1B).
130 Moreover, the grip strength of mutant mice was comparable with that of control mice (Fig. S1C).
131 The minimum Ferret diameter, which is the robust parameter in order to measure myofiber size,
132 and number of myofibers in BB and TA muscles remained unchanged in mutant mice (Fig. S1D,
133 E). As relayed signaling between mesenchymal progenitors and muscle stem (satellite) cells is
134 critical for muscle hypertrophy (21), we also quantified the number of muscle stem cells.
135 Immunofluorescence staining of Pax7, a marker of muscle stem cells (22), revealed no difference
136 in the number of muscle stem cells between control and mutant BB and TA muscles (Fig. S1F).
137 We next investigated the fiber types of slow soleus muscles, which are affected by muscle fiber-
138 and muscle stem cell-specific AR ablation (8, 23). Analysis of soleus muscles fiber types by
139 immunofluorescence staining of type I (Myh7), type IIa (Myh2), and type IIx/IIb (without
140 signals) muscle fibers demonstrated no difference in the fiber-type parameters (minimum Ferret
141 diameter and frequency of each fiber-type) between control and mutant mice (Fig. S1G, H).
142 Thus, AR expression loss in mesenchymal progenitors has a limited effect on the steady-state
143 limb muscles of young mice.
144
145

146 **The impact of AR deficiency in mesenchymal progenitors on adipogenesis in muscles was**
147 **limited**
148 We also examined the adipogenesis of mesenchymal progenitors in mutant mice because
149 adipocytes originate from mesenchymal progenitors in skeletal muscles (9). To address this, both
150 the control and mutant mice were subjected to an 8-week regimen of high fat diet (HFD) feeding
151 (Fig. S2A). No significant differences were observed between the control mice and mutant mice
152 in terms of total body weight, hindlimb muscle weights, epididymal white adipose tissue
153 (eWAT) mass, and subcutaneous white adipose tissue (sWAT) mass (Fig. S2B), and grip
154 strength (Fig. S2C). Immunofluorescence staining of perilipin, a marker of adipocytes (24),
155 along with laminin, demonstrated no significant difference in the minimum Ferret diameter of
156 myofibers or the area occupied by adipocytes between the control and mutant TA muscles (Fig.
157 S2D, E).
158 To further investigate the impact of AR deficiency in muscle adipogenesis, we employed
159 a muscle injury model by administering glycerol injections into the TA muscle of both control
160 and mutant mice (Fig. S2F). No significant differences were observed between the control and
161 mutant mice in terms of the body and TA muscle weights at 2 weeks after injection (Fig. S2G).
162 Immunofluorescence staining of perilipin in conjunction with laminin (Fig. S2H) revealed no
163 significant difference in the minimum Ferret diameter of myofibers or the area occupied by
164 adipocytes between the control and mutant TA muscles (Fig. S2I). These findings suggest that
165 the absence of AR in mesenchymal progenitors does not significantly affect the adipogenic
166 properties of TA muscles.
167
168

169 **AR deficiency in mesenchymal progenitors affected limb skeletal muscles in mature adult**
170 **but not aged mice**
171 To examine the long-term impact of AR ablation on mesenchymal progenitors, we analyzed
172 mature adult (6 months old) mice and compared the Cre control group and mutant group (Fig.
173 2A). In the mature adult mutant mice, we observed decreases in body weight, TA, and
174 gastrocnemius muscle weights (Fig. 2B), while there were no significant changes in the weights
175 of eWAT and sWAT (Fig. 2B), which are affected by systemic AR ablation (25). However, grip
176 strength (Fig. 2C) was comparable between the control and mutant mice.
177 Additionally, the weights of the entire body, hindlimb muscles, and white adipose tissues
178 were compared between aged (28 months old) control and mutant mice (Fig S2J). The aged
179 mutant mice did not exhibit any significant differences from the aged control mice (Fig. S2K and
180 S2L). Therefore, our findings demonstrate that AR deficiency in mesenchymal progenitors
181 affects skeletal muscle mass in mature adult mice only, not young or aged mice, primarily in the
182 limbs.
183
184 **Mesenchymal progenitor-specific AR ablation induced atrophy of LA/BC muscles**
185 The perineal LA/BC skeletal muscle complex exhibits increased responsiveness to androgens
186 compared with other striated muscles (26). Because this perineal muscle complex also has higher
187 AR expression (14), we examined the impact of AR ablation on mesenchymal progenitors of
188 LA/BC skeletal muscles. We confirmed efficient ablation of AR in PDGFRα+ cells in LA
189 muscles as well as limb muscles (Fig. 2D, E). At 14 weeks, 6 months, and 28 months of age, the
190 LA/BC mass was consistently lower in the mutant mice than control mice (Fig. 2F). Because AR
191 ablation in myofibers (*HSA-Cre;AR*$^{L2/Y}$ mice) also leads to reduced LA/BC mass (27), we

192 generated *HSA-Cre;PDGFRα-CreER;AR*$^{L2/Y}$ mice to examine whether the weight reduction
193 depended on AR in myofibers. Interestingly, the LA/BC weight was lower in *HSA-Cre;AR*$^{L2/Y}$
194 mice than in *PDGFRα-CreER;AR*$^{L2/Y}$ mice (Fig. 2G). Moreover, *HSA-Cre;PDGFRα-*
195 *CreER;AR*$^{L2/Y}$ mice had the lowest LA/BC mass compared with *HSA-Cre;AR*$^{L2/Y}$ and *PDGFRα-*
196 *CreER;AR*$^{L2/Y}$ mice (Fig. 2G). These findings suggest that AR expression in both myofibers and
197 mesenchymal progenitors independently regulates the mass of perineal muscles. We also found
198 that AR depletion in mesenchymal progenitors in LA muscles led to a decrease in the number of
199 PDGFRα+ cells (Fig. 2H). Examination of the cross-sectional area of LA muscles by laminin
200 staining (Fig. 2I) revealed a lower myofiber size in the mutant mice than control mice (Fig. 2J).
201 In summary, AR expression in mesenchymal progenitors independently regulates the mass of
202 perineal muscles, separate from its influence on myofibers.
203
204 **AR regulated genes related to extracellular matrix organization in mesenchymal**
205 **progenitors**
206 To determine the effects of AR on gene expression, we performed RNA-seq in PDGFRα+ cells
207 from the LA/BC muscles of both control and mutant mice (Fig. 3A). Using a previously
208 established gating strategy for isolating mesenchymal progenitors (CD45− CD31− Vcam1−
209 PDGFRα+) (12)(Fig. S3A), we isolated 300 PDGFRα+ cells from LA/BC muscles for RNA-seq.
210 We detected more than 100,000 genes in these cells, indicating sufficient read depth for further
211 analysis (Fig. S3B). The PCA plot showed separation between the control and mutant samples
212 (Fig. S3C). We identified 80 upregulated and 76 downregulated genes, including AR, in
213 PDGFRα+ cells from the mutant mice (Fig. S3D). The upregulated genes were enriched in the
214 Gene Ontology (GO) terms including regulation of cell death and cell motility (Fig. 3B). On the

215 other hand, the downregulated genes were enriched in the GO terms related to extracellular
216 matrix organization and regulation of proteolysis (Fig. 3C).
217 To determine the AR target genes, we used CUT&RUN method for AR and trimethylated
218 lysine 4 from histone H3 (H3K4me3), which is enrich in active promoters, in mesenchymal
219 progenitors isolated from C57BL/6J male mice treated with DHT 2 hours before sampling (Fig
220 3D). We detected total 6542 peaks of AR in mesenchymal progenitors in skeletal muscles. The
221 AR peaks were primarily distributed in intron or intergenic regions, similar to previous reports
222 with AR ChIP-seq in muscle and non-muscle tissues (28, 29). We also found the androgen
223 response elements (ARE) in these peaks as the most enriched motif as well as AR half-site (Fig.
224 3E, S3F). Moreover, AR CUT&RUN was validated by peaks found in the *Fkbp5* locus (Fig.
225 S3G), where canonical AR binding sites are located for several tissues (28). By profiling AR
226 peaks with AR and H3K4me3 reads, we found that AR binding sites were present mainly not in
227 promoter region (Fig. 3F). Furthermore, AR binding events were enriched for regulation of
228 locomotion and extracellular matrix organization GO terms (Fig. 3G). These results indicate that
229 AR in mesenchymal progenitors directly regulate the transcriptions including extracellular
230 matrix organization genes.
231
232 **AR in mesenchymal progenitors regulated Igf1 expression**
233 To further investigate the gene regulation by AR in mesenchymal progenitors, we combined the
234 RNA-seq and CUT&RUN analysis. We found 39 genes which were downregulated in AR-
235 deficient mesenchymal progenitors and have AR peaks annotated by a nearest transcription start
236 sites (TSS) analysis (Fig. 4A). Top enriched GO term of these genes was extracellular matrix
237 organization (Fig. 4B), including Collagen family (*Col1a1*, *Col3a1*, *Col4a1*, *Col4a2*, *Col5a1*,

238 *Col5a2*, and *Col6a2*, Fig. S4A and S4B), and *Igf1* (Fig. 4C), which is critical for maintaining
239 muscle mass (30). We also found the bindings of AR with ARE and peaks of H3K4me3 in
240 upstream of *Igf1* TSS (Fig. 4D). Moreover, AR peaks were found with ARE in *Ar* gene locus
241 (Fig. S4C), indicating the regulation of *Ar* by AR in mesenchymal progenitors as other cells (31).
242 To further investigate the effects of androgen and AR on *Igf1* expression, we isolated PDGFRα+
243 cells from C57BL/6J male mice treated with DHT (Fig. 4E). *Igf1* expression was upregulated in
244 PDGFRα+ cells after DHT administration (Fig. 4F). We also found reduction of IGF1 protein in
245 the mutant LA muscles (Fig. 4G and 4H). Taken together, AR in mesenchymal progenitors
246 regulates *Igf1* expression controlling skeletal muscle mass.

247 **Discussion**

248 In the present study, we demonstrated that mice with specific AR ablation in mesenchymal
249 progenitors showed lower skeletal muscle mass in the limbs only at the mature adult stage, but
250 not at a younger stage (14 weeks old). Taken together with previous reports demonstrating that
251 mice with AR ablation specifically in fast-twitch fibers lack muscle mass reduction at 13 weeks
252 old but exhibit this reduction at 12–13 months old (23), there may be a potential age-dependent
253 role of AR or an effect that requires time to develop. Additionally, we demonstrated that the
254 number of Pax7+ muscle stem cells was similar between adult control and mutant mice. This is
255 in contrast to the observed reduction in myoblast proliferation following deletion of AR in the
256 mesenchyme of BC muscles during development (16), providing evidence that AR in
257 mesenchymal progenitors plays distinct roles during development, adulthood, and aging in mice.
258 We also showed that specific ablation of AR in mesenchymal progenitors does not affect the
259 fiber types of slow-twitch muscles. Depletion of mesenchymal progenitors results in a slight
260 increase in the proportion of slow fibers (type I) predominantly in fast-twitch TA muscles (12),
261 suggesting that factors other than AR in mesenchymal progenitors influence muscle fiber types.

262 PDGFRα+ cells are the origin of ectopic adipocytes in skeletal muscles (9, 10). However,
263 the specific molecular mechanisms underlying fatty infiltration of muscles remain largely
264 unexplored (32). In general, androgen and AR signaling seem to have inhibitory effects on
265 adipogenesis (33). Serum androgens are linked to reduced levels of fatty infiltration of skeletal
266 muscles (34). In contrast, deprivation of androgens leads to an increase in fatty infiltration of
267 skeletal muscle in men (35). Moreover, transgenic mice expressing AR induced by collagen type
268 I alpha 1, which is also expressed in mesenchymal progenitors (36), have reduced body weight
269 and fat mass (37). Additionally, HFD-induced fat mass deposition in skeletal muscles was

270 increased by a low androgen level caused by orchiedectomy (38). However, our results indicate
271 that AR deficiency in mesenchymal progenitors does not affect adipogenesis in skeletal muscle
272 even after HFD feeding or glycerol injection. An indirect androgen pathway may also regulate
273 adipogenesis of mesenchymal progenitors in skeletal muscles. Indeed, recent research indicates
274 that androgens can modulate macrophage polarization, subsequently affecting adipocyte
275 differentiation (39). Further studies are needed to gain a comprehensive understanding of the
276 mechanisms by which androgens and AR signaling influence fatty infiltration of muscle.

277 We observed a modest reduction in the muscle weight of the mutant mice at the mature
278 adult age (24 weeks old), but this effect was not observed in aged mice (28 months old). Because
279 selective ablation of AR in myofibers does not lead to reduced muscle mass even in 40-week-old
280 mice (27), the role of AR in mesenchymal progenitors is more important than its role in
281 myofibers in the context of muscle maintenance, at least at the mature adult age. A decrease in
282 testosterone concentration, even in 1-year-old mice compared with young 12-week-old mice
283 (40), may contribute to muscle mass loss, potentially masking any subtle differences between the
284 aged control and mutant mice. Due to the reduction in muscle mass observed in 2-year-old mice
285 with AR depletion specifically in fast-twitch fibers (23), AR expression in muscle fibers may
286 play a crucial role in regulating muscle metabolism and quality, which help maintain muscle
287 mass in aged mice.

288 The perineal skeletal muscles LA and BC are highly androgen sensitive. Muscle fiber-
289 specific AR knockout results in a more pronounced mass reduction in LA/BC muscles compared
290 with limb muscles (26, 27), which is consistent with our present study demonstrating a consistent
291 reduction in LA/BC muscles in mice with AR ablation in mesenchymal progenitors. We also
292 demonstrated that AR deficiency in mesenchymal progenitors resulted in reduced LA/BC

293 weight, although the extent of the reduction was milder compared with mice in which AR was
294 ablated in muscle fibers. Furthermore, the double Cre mice (*HSA-Cre;PDGFRα-CreER;AR*$^{L2/Y}$),
295 with ablation of AR in both myofibers and mesenchymal progenitors, exhibited a greater
296 reduction in LA/BC mass compared with single Cre mice (*HSA-Cre;AR*$^{L2/Y}$ or *PDGFRα-*
297 *CreER;AR*$^{L2/Y}$). Taken together, AR expression in mesenchymal progenitors independently
298 regulates the mass of perineal muscles, separate from the influence of AR in myofibers. The
299 distinct reactions observed in perineal and limb muscles could be attributed to a greater
300 abundance of myonuclei expressing AR in perineal muscles compared with limb muscles (14).
301 Nevertheless, our findings revealed that the majority of PDGFRα+ cells exhibited AR expression
302 in both limb and perineal muscles, suggesting an additional mechanism by which AR in
303 mesenchymal progenitors regulates muscle mass and other mesenchymal progenitor functions.
304 The signaling pathway involving IGF1 plays a crucial role in both the developmental
305 growth and steady-state maintenance of skeletal muscle mass (41, 42). IGF1 is produced
306 primarily in the liver (43) but local production, including in skeletal muscles, is induced by
307 androgen treatment. The administration of testosterone to older men led to an increase in IGF1
308 protein expression in the limb (vastus lateralis) muscles (44). *Igf1* expression is decreased in the
309 LA/BC muscles of mice with skeletal muscle-specific AR ablation (27). Dubois et al. has
310 reported indirect androgen regulation of IGF1 via non myocytic AR because Myod-Cre-driven
311 AR-deficient mice showed no reduction in the *Igf1* transcript level, and *Igf1* expression was
312 decreased after castration in skeletal muscles (17). We demonstrated that AR in mesenchymal
313 progenitors in skeletal muscles regulated *Igf1* expression, governing muscle mass. Moreover,
314 activation of Akt signaling via the expression of Bmp3b in mesenchymal progenitors (12)

315 suggests a connection with Igf1, highlighting the complex interplay of signaling pathways in the
316 maintenance of skeletal muscle mass.

317 In summary, our results show that AR in mesenchymal progenitors regulates skeletal
318 muscle mass via Igf1 expression. Combining treatment with androgens and IGF1 could be useful
319 to treat muscle atrophy such as sarcopenia.

320 **Materials and Methods**

321 **Animals**

322 *PDGFRα-CreER* mice (19), *HSA-Cre* mice (45), and C57BL/6J male mice were purchased from
323 Jackson Laboratories (Strain #: 018280, 006149, and 000664, respectively). $AR^{L2/Y}$ mice have
324 been described (20). *PDGFRα-CreER* male mice were crossed with $AR^{L2/+}$ female mice to
325 generate *PDGFRα-CreER;*$AR^{L2/Y}$ male mutant mice. Male littermates with the *PDGFRα-*
326 *CreER;*$AR^{+/Y}$ genotype were used as control mice. To generate *HSA-Cre;PDGFRα-CreER;*$AR^{L2/Y}$
327 male mice, *HSA-Cre* male mice were crossed with *PDGFRα-CreER;*$AR^{L2/+}$ female mice. All
328 mice were housed in a specific pathogen-free facility under climate-controlled conditions and a
329 12-hour light/dark cycle and were provided water and a standard diet *ad libitum*. In both control
330 and mutant mice, 100 μL of 20 mg/mL tamoxifen (TMX, Sigma-Aldrich, Cat# T5648),
331 dissolved in corn oil (Sigma-Aldrich, Cat# C8267), was injected intraperitoneally for 5
332 consecutive days at 8 or 12 weeks of age. A high-fat diet (HFD, CLEA Japan, Cat# HFD32) was
333 given *ad libitum* for 8 weeks to induce obesity in mice. The diet was refreshed every 2 days. To
334 induce fatty infiltration of skeletal muscle, 100 μL of 50% v/v glycerol was injected into tibialis
335 anterior (TA) muscles under anesthesia using isoflurane (46). To induce AR signaling,
336 dihydrotestosterone (DHT or stanolone, 2.5 mg/mouse; Tokyo Chemical Industry, Cat# A0462),
337 dissolved in absolute ethanol and diluted in 0.3% w/v hydroxypropyl cellulose (Wako, Cat# 085-
338 07932) in PBS, was injected subcutaneously at 2 hours before sampling. All animal experiments
339 were approved by the Animal Experiment Committee of Ehime University (Approval No. 37A1-
340 1·16) and were conducted in full compliance with the Guidelines for Animal Experiments at
341 Ehime University.

342

343 **Grip strength**

344 The grip strength of the forelimb was measured using a strain gauge (Melquest, Cat# GPM-
345 100B). The maximal force was determined after 10 measurements. The mean value recorded by
346 two independent experimenters was reported as the grip strength of each mouse.

347

348 **Immunofluorescence staining and microscopy**

349 For immunofluorescence staining, muscles were snap frozen in liquid nitrogen-chilled
350 isopentane. Cryosections of 10 μm thickness were prepared for immunofluorescence staining.
351 Sections were fixed in 4% paraformaldehyde in PBS for 5 min, blocked in 5% goat serum
352 (Gibco, Cat# 16210-064) in PBS for 60 min, and incubated with primary antibodies overnight at
353 4°C. For staining of myosin heavy chain (Myh), sections were air-dried and blocked with
354 M.O.M. reagent (Vector Laboratories, Cat# MKB-2213-1) at room temperature for 60 min.
355 Primary antibodies for Myh diluted in 1% BSA/PBS were incubated at 37°C for 45 min. The
356 antibodies used for immunofluorescence staining were anti-AR (Abcam, Cat# ab108341,
357 RRID:AB_10865716; 1/100), anti-PDGFRA (R&D Systems, Cat# AF1062,
358 RRID:AB_2236897; 1/80), anti-Laminin α2 (Santa Cruz Biotechnology, Cat# sc-59854,
359 RRID:AB_784266; 1/400), anti-Pax7 (DSHB, Cat# PAX7, RRID:AB_528428; 1/5), anti-
360 Laminin (Sigma-Aldrich, Cat# L9393, RRID:AB_477163; 1/500), anti-Myh7 (DSHB, Cat# BA-
361 D5, RRID:AB_2235587, supernatant; 1/100), anti-Myh2 (DSHB, Cat# SC-71,
362 RRID:AB_2147165, supernatant; 1/100), anti-Perilipin (Sigma-Aldrich, Cat# P1873,
363 RRID:AB_532267; 1/250), Alexa fluor 488 goat anti-rabbit IgG (Thermo Fisher Scientific, Cat#
364 A-11008; RRID:AB_143165; 1/1000), Alexa fluor 555 donkey anti-goat IgG (Thermo Fisher
365 Scientific, Cat# A-21432, RRID:AB_2535853; 1/1000), Alexa fluor 647 goat anti-rat IgG

366 (Thermo Fisher Scientific, Cat# A-21247, RRID:AB_141778; 1/1000), Alexa fluor 568 goat
367 anti-mouse IgG1 (Thermo Fisher Scientific, Cat# A-21124, RRID: AB_2535766; 1/1000), Alexa
368 fluor 488 goat anti-mouse IgG2b (Thermo Fisher Scientific, Cat# A-21141, RRID:AB_2535778;
369 1/1000), Alexa fluor 568 goat anti-rabbit IgG (Thermo Fisher Scientific, Cat# A-11011,
370 RRID:AB_143157; 1/1000), and Alexa fluor 647 goat anti-rabbit IgG (Thermo Fisher Scientific,
371 Cat# A27040; RRID:AB_143165; 1/1000). Nuclei were counterstained with DAPI. Entire cross
372 sections of fluorescence images were photographed using BIOREVO (Keyence) or Axio
373 Observer7 (Zeiss).
374

375 **Quantification of muscle sections**

376 To quantify the number, cross-sectional area (CSA), and minimum Ferret diameter of the
377 myofibers, captured images of entire cross sections were analyzed using Fiji (v2.3.0)
378 (https://imagej.net/Fiji). The myofiber area was identified by the laminin+ signals. The region of
379 interest (ROI) was set within the laminin+ areas. The frequency of each muscle fiber type in the
380 ROI was recorded by Trainable Weka Segmentation in Fiji after manual training. Small (< 150
381 μm^2) or large (> 10,000 μm^2) fibers were excluded for analyzing. The number of AR+PDGFRα+
382 mesenchymal progenitors, Pax7+ satellite cells, and the perilipin+ area was manually counted or
383 measured using Fiji.
384

385 **Isolation of mesenchymal progenitors from skeletal muscle**

386 Isolation of mononuclear cells from muscle was performed as described previously (47) with
387 minor modifications. Briefly, muscles were chopped in PBS on ice and digested using 800 U/mL
388 collagenase type 2 (Worthington, Cat# LS004177) in F10 medium (Gibco, Cat# 11550-043)

389 supplemented with 10% horse serum (Gibco, Cat# 26050-088) and antibiotic–antimycotic
390 (Gibco, Cat# 15240-062) for 60 min. Another digestion was conducted using 1000 U/mL
391 collagenase type 2 and 11 U/mL dispase (Gibco, Cat# 17105-041) for 30 min. The supernatants
392 were transferred to a 40 μm cell strainer (Falcon, Cat# 352340) to filter the debris and then
393 centrifuged to yield a cell suspension. The following antibodies were used: FITC anti-CD31
394 (BioLegend, Cat# 102406; RRID:AB_312901; 1/100), FITC anti-CD45 (BioLegend, Cat#
395 103108, RRID:AB_312973; 1/100), PE anti-VCAM1 (Thermo Fisher Scientific, Cat# 12-1061-
396 82, RRID:AB_2572573; 1/100), and APC anti-PDGFRα (R&D Systems, Cat# FAB1062A,
397 RRID:AB_3073817; 1/30). The BD FACSAria II (RRID:SCR_018091) or BD FACSAria
398 Fusion (BD Biosciences) was used for fluorescence-activated cell sorting, and the plot was
399 analyzed by FlowJo v10.1r7 (BD Life Sciences, RRID:SCR_008520).
400
401 **RNA-seq and data analysis**
402 For isolation of RNA from mesenchymal progenitors in LA/BC muscles, 300 PDGFRα+ cells
403 were sorted into the wells of a 96-well plate containing 10 μL lysis buffer at 4°C. The lysis
404 buffer was prepared by mixing 1 μL RNase inhibitor (TaKaRa, Cat# 2313A) and 19 μL 10X
405 lysis buffer (TaKaRa, Cat# 635013) diluted to 1X with nuclease-free water. 3' UTR RNA-seq
406 was conducted using the CEL-Seq2 protocol (48), with the exception of employing the Second
407 Strand Synthesis Module (New England Biolabs, Cat# E6111L) for double-stranded cDNA
408 synthesis. The library was then amplified via 10 cycles of PCR without any sample pooling.
409 Subsequently, the library was sequenced on the Illumina NovaSeq 6000, and quantitative
410 analysis was performed using 81 bp of insert reads (Read2).

411 Cell barcode and UMI information from Read1 were extracted using UMI-tools (v1.1.2)
412 (49) with the following command: "umi_tools extract -I read1.fastq --read2-in=read2.fastq --bc-
413 pattern=NNNNNNNNNNCCCCCCCC". Adaptor and low-quality sequences were removed,
414 and reads with a length less than 20 bp were discarded using TrimGalore (v0.6.7;
415 http://www.bioinformatics.babraham.ac.uk/projects/trim_galore/). The processed reads were then
416 mapped to the GRCm38 reference genome using HISAT2 (v2.2.1) (50). Read counts for each
417 gene were obtained using featureCounts (v2.0.1) (51), and UMI duplications were removed
418 using UMI-tools. Four cell barcodes, "ATGCAATGC," "GACACGACA," "CGATGCGAT,"
419 and "TCTGGTCTG," were assigned to each sample. Differentially expressed genes were
420 identified using DESeq2 (v1.36.0) (52) with thresholds of |log2FC| > 1 and padj < 0.1.
421 Metascape (53) was used for Gene Ontology (GO) enrichment analysis.
422
423 **CUT&RUN and data analysis**
424 C57BL/6J male mice (10-12 weeks old) were treated with DHT at 2 hours before sampling for
425 FACS. For isolation of chromatin from mesenchymal progenitors in hindlimbs muscles, 500,000
426 PDGFRα+ cells were sorted to 20%FBS, DMEM/F12 (Gibco, Cat# 10565-018), Ultroser G
427 (Pall, Cat# 15950-017) supplemented with DHT (100 nM) to activate AR signaling during
428 sorting. After sorting, the nuclei were prepared with ChIC/CUT&RUN Assay Kit (Active Motif,
429 Cat# 53180) following the manufacturer's protocol. For AR (n = 4), H3K4me3 (n = 2), and IgG
430 control (n = 2) CUT&RUN, the following antibodies (1 µg/reaction) were used: anti-AR
431 (Abcam, Cat# ab108341, RRID:AB_10865716), anti-H3K4me3 (Active Motif, Cat# 39916,
432 RRID:AB_2687512), and rabbit negative control IgG (Active Motif, part of Cat# 53180). To
433 obtain enriched DNA after the CUT&RUN reaction, 20 µL of DNA purification elution buffer

434 was used instead of 55. The library was prepared using NEBNext Ultra II for DNA Library
435 Preparation for Illumina (New England Biolabs, Cat# E7645L) with some modifications
436 according to the Active Motif's instruction. All reactions were performed by half volume.
437 Constructed libraries were analyzed by 2100 Bioanalzyer using High Sensitivity DNA kit
438 (Agilent Technologies, Cat# 5067-4626), and quantified by qPCR using KAPA Library
439 Quantification Kits (Kapa Biosystems, Cat# KK4824). The library was sequenced on the
440 Illumina NovaSeq 6000 for 51 cycles of paired-end sequencing.

441 Paired-end reads were trimmed with Trim Galore and mapped to mm10 using Bowtie2
442 (v2.4.5) (54) with the following options: --no-mixed --no-discordant. Multi or no mate reads
443 were removed with samtools (v1.10) (55) view (-q 4 -F 0x2). To identify AR peaks across
444 samples, BAM files were merged across biological replicates (n = 2) to call peaks with MACS2
445 (v2.2.7.1) (-q 0.05) (56). H3K4me3 peaks were called on individual BAM files using MACS2 (-
446 q 0.0001). Merged BAM files for AR and IgG were used for downstream analysis (2 merged
447 BAM files for AR and 1 merged BAM file for IgG). Motif enrichment analysis of AR peaks was
448 performed with HOMER (v4.11) (57) findMotifs with -size 200 -mask options and AR peaks
449 were annotated to mm10 genes using annotatePeaks (-size 200 -mask) from MACS2 summit
450 files. Peaks distribution was annotated on mm10 (TxDb.Mmusculus.UCSC.mm10.knownGene,
451 R package version 3.4.7.) using ChIPpeakAnno package (v3.30.1) (58, 59) with MACS2
452 narrowPeak files. Promoter region was defined as 2000 bp upstream to 500 bp downstream of
453 transcription start sites (TSS). Common AR peaks-associated genes between replicates were
454 identified with Venn diagrams tools (http://bioinformatics.psb.ugent.be/webtools/Venn/). GO
455 enrichment analysis of common AR peaks-associated genes for GO Biological Process was
456 performed with Metascape. To generate bigwig files, merged (AR or IgG) or individual

457 (H3K4me3) BAM files were converted to CPM-normalized bigwig files using deepTools
458 (v3.5.1) (60) bamCoverage (--binSize 100 --normalizeUsing CPM). Peaks were visualized using
459 Integrative Genomics Viewer (IGV, v2.12.3) (61) with bigwig files. A count matrix for
460 aggregation plot was generated by deepTools computeMatrix reference-point (--skipZeros) with
461 AR and H3K4me3 bigwig files. Heatmaps were generated with count matrix files using
462 deepTools plotHeatmap.
463
464 **RNA isolation and quantitative real-time PCR**
465 Total RNA was extracted from freshly sorted 30,000 PDGFRα+ cells from LA/BC muscles
466 using the RNeasy Plus Micro Kit (Qiagen, Cat# 74034) following the manufacturer's protocol.
467 Reverse transcription was performed using PrimeScript (Takara, Cat# RR036A) to synthesize
468 cDNA from total RNA. Quantitative PCR (qPCR) was conducted in technical duplicate samples
469 utilizing TB Green Premix Ex Taq II (Takara, Cat# RR820S) and the Thermal Cycler Dice
470 (Takara, Cat# TP850). The expression levels of the target genes were normalized to that of
471 *Rpl13a*. The primer sequences are listed in Table S1.
472
473 **Western blotting**
474 LA muscles were dissolved in RIPA buffer (Fujifilm, Cat# 182–02451) supplemented with
475 protease inhibitors (Nacalai Tesque, Cat# 25955-11). Tissue-extracts were separated by SDS-
476 PAGE and transferred to polyvinylidene fluoride membranes. The membranes were blocked with
477 5% skim milk in TBS with Tween-20 (PBST), followed by incubation with anti-IGF1 (R&D
478 Systems, Cat# AF791, RRID:AB_2248752; 1/2000) or anti-GAPDH antibodies (Cell Signaling
479 Technology, Cat# 5174, RRID: AB_10622025; 1/1000) overnight at 4°C. The membranes were

480 incubated with an anti-goat (Agilent, Cat# P0160, 1:5000) or anti-rabbit immunoglobulin/HRP
481 secondary antibody (Agilent, Cat# P0448, RRID: AB_2617138; 1:5000) for 60 min at room
482 temperature. Signals were detected using ECL Prime Western Blotting Detection Reagents
483 (Amersham, Cat# RPN2232) on the Image Quant LAS 4000 system (GE Healthcare). Band
484 images were quantified by Fiji.
485
486 **Statistical analysis**
487 Prism 9 (GraphPad Software) or R (v4.0.5) (https://www.r-project.org) was used for the
488 statistical analysis. Welch's t-test was used to compare two groups. The two-sample test for
489 equality of proportions was performed using the test of equal or given proportions. To compare
490 variables among three or more groups, Brown-Forsythe and Welch's ANOVA test with
491 Dunnett's T3 multiple comparison test was used.

492 **Acknowledgments**

493 We are grateful to A. Nishio and Y. Sato for their technical support. We thank Y. Tanaka for the
494 flow cytometry support, N. Tokunaga for the library preparations, and other members of the
495 Division of Medical Research Support, the Advanced Research Support Center, Ehime
496 University. This study was partly performed in the Cooperative Research Project Program in the
497 Medical Institute of Bioregulation (MIB), Kyushu University. We also thank the Medical
498 Research Center for High Depth Omics, MIB, Kyushu University for the sequencing, and RIST
499 at Kyushu University for the high-performance computing.

500 **Data Availability**

501 RNA-seq and CUT&RUN data have been deposited and are publicly available in the Gene

502 Expression Omnibus as accession number GSE247378.

503 **References**

504

505 1. G. N. Papanicolaou, E. A. Falk, General Muscular Hypertrophy Induced by Androgenic
506 Hormone. *Science* **87**, 238–239 (1938).

507 2. S. Bhasin, *et al.*, The Effects of Supraphysiologic Doses of Testosterone on Muscle Size and
508 Strength in Normal Men. *N. Engl. J. Med.* **335**, 1–7 (1996).

509 3. D. B. Lubahn, *et al.*, Cloning of Human Androgen Receptor Complementary DNA and
510 Localization to the X Chromosome. *Science* **240**, 327–330 (1988).

511 4. A. M. Lincoff, *et al.*, Cardiovascular Safety of Testosterone-Replacement Therapy. *N. Engl. J.*
512 *Med.* **389**, 107–117 (2023).

513 5. H. E. MacLean, *et al.*, Impaired skeletal muscle development and function in male, but not
514 female, genomic androgen receptor knockout mice. *FASEB J.* **22**, 2676–2689 (2008).

515 6. I. Sakakibara, *et al.*, Myofiber androgen receptor increases muscle strength mediated by a
516 skeletal muscle splicing variant of Mylk4. *iScience* **24**, 102303 (2021).

517 7. H. Sakai, T. Sato, M. Kanagawa, S. Fukada, Y. Imai, Androgen receptor in satellite cells is not
518 essential for muscle regenerations. *Exp. Results* **1** (2020).

519 8. V. Dubois, *et al.*, A satellite cell-specific knockout of the androgen receptor reveals myostatin
520 as a direct androgen target in skeletal muscle. *FASEB J.* **28**, 2979–2994 (2014).

521 9. A. Uezumi, S. Fukada, N. Yamamoto, S. Takeda, K. Tsuchida, Mesenchymal progenitors
522 distinct from satellite cells contribute to ectopic fat cell formation in skeletal muscle. *Nat. Cell*
523 *Biol.* **12**, 143–152 (2010).

524 10. A. W. B. Joe, *et al.*, Muscle injury activates resident fibro/adipogenic progenitors that
525 facilitate myogenesis. *Nat. Cell Biol.* **12**, 153–163 (2010).

526 11. M. N. Wosczyna, *et al.*, Mesenchymal Stromal Cells Are Required for Regeneration and
527 Homeostatic Maintenance of Skeletal Muscle. *Cell Rep.* **27**, 2029-2035.e5 (2019).

528 12. A. Uezumi, *et al.*, Mesenchymal Bmp3b expression maintains skeletal muscle integrity and
529 decreases in age-related sarcopenia. *J. Clin. Investig.* **131** (2020).

530 13. A. Uezumi, *et al.*, Fibrosis and adipogenesis originate from a common mesenchymal
531 progenitor in skeletal muscle. *J. Cell Sci.* **124**, 3654–3664 (2011).

532 14. J. A. Johansen, S. M. Breedlove, C. L. Jordan, Androgen Receptor Expression in the Levator
533 Ani Muscle of Male Mice. *J. Neuroendocr.* **19**, 823–826 (2007).

534 15. I. Sinha-Hikim, W. E. Taylor, N. F. Gonzalez-Cadavid, W. Zheng, S. Bhasin, Androgen
535 Receptor in Human Skeletal Muscle and Cultured Muscle Satellite Cells: Up-Regulation by
536 Androgen Treatment. *J. Clin. Endocrinol. Metab.* **89**, 5245–5255 (2004).

537 16. L. A. Ipulan, *et al.*, Nonmyocytic Androgen Receptor Regulates the Sexually Dimorphic
538 Development of the Embryonic Bulbocavernosus Muscle. *Endocrinology* **155**, 2467–2479
539 (2014).

540 17. V. Dubois, *et al.*, Enobosarm (GTx-024) Modulates Adult Skeletal Muscle Mass
541 Independently of the Androgen Receptor in the Satellite Cell Lineage. *Endocrinology* **156**, 4522–
542 4533 (2015).

543 18. M. Kanou, *et al.*, Polyamine pathway is associated with muscle anabolic effects by androgen
544 receptor ligand. *JCSM Rapid Commun.* **4**, 57–74 (2021).

545 19. S. H. Kang, M. Fukaya, J. K. Yang, J. D. Rothstein, D. E. Bergles, NG2+ CNS Glial
546 Progenitors Remain Committed to the Oligodendrocyte Lineage in Postnatal Life and following
547 Neurodegeneration. *Neuron* **68**, 668–681 (2010).

548 20. T. Matsumoto, K. Takeyama, T. Sato, S. Kato, Androgen receptor functions from reverse
549 genetic models. *J. Steroid Biochem. Mol. Biol.* **85**, 95–99 (2003).

550 21. A. Kaneshige, *et al.*, Relayed signaling between mesenchymal progenitors and muscle stem
551 cells ensures adaptive stem cell response to increased mechanical load. *Cell Stem Cell* **29**, 265-
552 280.e6 (2022).

553 22. P. Seale, *et al.*, Pax7 Is Required for the Specification of Myogenic Satellite Cells. *Cell* **102**,
554 777–786 (2000).

555 23. T. Hosoi, *et al.*, Sarcopenia phenotype and impaired muscle function in male mice with fast-
556 twitch muscle-specific knockout of the androgen receptor. *Proc. Natl. Acad. Sci.* **120**,
557 e2218032120 (2023).

558 24. A. S. Greenberg, *et al.*, Perilipin, a major hormonally regulated adipocyte-specific
559 phosphoprotein associated with the periphery of lipid storage droplets. *J. Biol. Chem.* **266**,
560 11341–11346 (1991).

561 25. W. Fan, *et al.*, Androgen Receptor Null Male Mice Develop Late-Onset Obesity Caused by
562 Decreased Energy Expenditure and Lipolytic Activity but Show Normal Insulin Sensitivity With
563 High Adiponectin Secretion. *Diabetes* **54**, 1000–1008 (2005).

564 26. J. Ophoff, *et al.*, Androgen Signaling in Myocytes Contributes to the Maintenance of Muscle
565 Mass and Fiber Type Regulation But Not to Muscle Strength or Fatigue. *Endocrinology* **150**,
566 3558–3566 (2009).

567 27. C. Chambon, *et al.*, Myocytic androgen receptor controls the strength but not the mass of
568 limb muscles. *Proc. Natl. Acad. Sci.* **107**, 14327–14332 (2010).

569 28. P. Pihlajamaa, *et al.*, Tissue-specific pioneer factors associate with androgen receptor
570 cistromes and transcription programs. *EMBO J.* **33**, 312–326 (2014).

571 29. K. Ghaibour, *et al.*, Androgen receptor coordinates muscle metabolic and contractile
572 functions. *J. Cachexia, Sarcopenia Muscle* **14**, 1707–1720 (2023).

573 30. C. Rommel, *et al.*, Mediation of IGF-1-induced skeletal myotube hypertrophy by
574 PI(3)K/Akt/mTOR and PI(3)K/Akt/GSK3 pathways. *Nat. Cell Biol.* **3**, 1009–1013 (2001).

575 31. J. M. Grad, L. S. Lyons, D. M. Robins, K. L. Burnstein, The Androgen Receptor (AR)
576 Amino-Terminus Imposes Androgen-Specific Regulation of AR Gene Expression via an Exonic
577 Enhancer. *Endocrinology* **142**, 1107–1116 (2001).

578 32. M. W. Hamrick, M. E. McGee-Lawrence, D. M. Frechette, Fatty Infiltration of Skeletal
579 Muscle: Mechanisms and Comparisons with Bone Marrow Adiposity. *Front. Endocrinol.* **7**, 69
580 (2016).

581 33. J. Rizk, R. Sahu, D. Duteil, An overview on androgen-mediated actions in skeletal muscle
582 and adipose tissue. *Steroids* **199**, 109306 (2023).

583 34. I. Miljkovic, *et al.*, Bioactive androgens and glucuronidated androgen metabolites are
584 associated with subcutaneous and ectopic skeletal muscle adiposity among older black men.
585 *Metabolism* **60**, 1178–1185 (2011).

586 35. D. Chang, *et al.*, Effect of androgen deprivation therapy on muscle attenuation in men with
587 prostate cancer. *J. Med. Imaging. Radiat. Oncol.* **58**, 223–228 (2014).

588 36. M. A. Chapman, K. Mukund, S. Subramaniam, D. Brenner, R. L. Lieber, Three distinct cell
589 populations express extracellular matrix proteins and increase in number during skeletal muscle
590 fibrosis. *Am. J. Physiol. Cell Physiol.* **312**, C131–C143 (2017).

591 37. A. A. Semirale, X. Zhang, K. M. Wiren, Body composition changes and inhibition of fat
592 development in vivo implicates androgen in regulation of stem cell lineage allocation. *J. Cell.*
593 *Biochem.* **112**, 1773–1786 (2011).

594 38. V. Dubois, *et al.*, Androgen Deficiency Exacerbates High-Fat Diet-Induced Metabolic
595 Alterations in Male Mice. *Endocrinology* **157**, 648–665 (2016).

596 39. X. Ren, *et al.*, Testosterone regulates 3T3-L1 pre-adipocyte differentiation and epididymal
597 fat accumulation in mice through modulating macrophage polarization. *Biochem. Pharmacol.*
598 **140**, 73–88 (2017).

599 40. M. E. Nilsson, *et al.*, Measurement of a Comprehensive Sex Steroid Profile in Rodent Serum
600 by High-Sensitive Gas Chromatography-Tandem Mass Spectrometry. *Endocrinology* **156**, 2492–
601 2502 (2015).

602 41. B. T. O'Neill, *et al.*, Insulin and IGF-1 receptors regulate FoxO-mediated signaling in muscle
603 proteostasis. *J. Clin. Invest.* **126**, 3433–3446 (2016).

604 42. F. Ascenzi, *et al.*, Effects of IGF-1 isoforms on muscle growth and sarcopenia. *Aging Cell*
605 **18**, e12954 (2019).

606 43. R. D. Kineman, M. del Rio-Moreno, A. Sarmento-Cabral, 40 YEARS of IGF1:
607 Understanding the tissue-specific roles of IGF1/IGF1R in regulating metabolism using the
608 Cre/loxP system. *J. Mol. Endocrinol.* **61**, T187–T198 (2018).

609 44. A. A. Ferrando, *et al.*, Testosterone administration to older men improves muscle function:
610 molecular and physiological mechanisms. *Am. J. Physiol. Endocrinol. Metab.* **282**, E601–E607
611 (2002).

612 45. P. Miniou, *et al.*, Gene targeting restricted to mouse striated muscle lineage. *Nucleic Acids*
613 *Res.* **27**, e27–e30 (1999).

614 46. N. Arsic, *et al.*, Vascular endothelial growth factor stimulates skeletal muscle regeneration in
615 Vivo. *Mol. Ther.* **10**, 844–854 (2004).

616 47. L. Liu, T. H. Cheung, G. W. Charville, T. A. Rando, Isolation of skeletal muscle stem cells
617 by fluorescence-activated cell sorting. *Nat. Protoc.* **10**, 1612–1624 (2015).

618 48. T. Hashimshony, *et al.*, CEL-Seq2: sensitive highly-multiplexed single-cell RNA-Seq.
619 *Genome Biol.* **17**, 77 (2016).

620 49. T. Smith, A. Heger, I. Sudbery, UMI-tools: modeling sequencing errors in Unique Molecular
621 Identifiers to improve quantification accuracy. *Genome Res.* **27**, 491–499 (2017).

622 50. D. Kim, J. M. Paggi, C. Park, C. Bennett, S. L. Salzberg, Graph-based genome alignment and
623 genotyping with HISAT2 and HISAT-genotype. *Nat. Biotechnol.* **37**, 907–915 (2019).

624 51. Y. Liao, G. K. Smyth, W. Shi, featureCounts: an efficient general purpose program for
625 assigning sequence reads to genomic features. *Bioinformatics* **30**, 923–930 (2014).

626 52. M. I. Love, W. Huber, S. Anders, Moderated estimation of fold change and dispersion for
627 RNA-seq data with DESeq2. *Genome Biol.* **15**, 550 (2014).

628 53. Y. Zhou, *et al.*, Metascape provides a biologist-oriented resource for the analysis of systems-
629 level datasets. *Nat. Commun.* **10**, 1523 (2019).

630 54. B. Langmead, S. L. Salzberg, Fast gapped-read alignment with Bowtie 2. *Nat. Methods* **9**,
631 357–359 (2012).

632 55. P. Danecek, *et al.*, Twelve years of SAMtools and BCFtools. *GigaScience* **10**, giab008
633 (2020).

634 56. Y. Zhang, *et al.*, Model-based analysis of ChIP-Seq (MACS). *Genome Biol.* **9**, R137 (2008).

635 57. S. Heinz, *et al.*, Simple Combinations of Lineage-Determining Transcription Factors Prime
636 cis-Regulatory Elements Required for Macrophage and B Cell Identities. *Mol. Cell* **38**, 576–589
637 (2010).

638 58. L. J. Zhu, *et al.*, ChIPpeakAnno: a Bioconductor package to annotate ChIP-seq and ChIP-
639 chip data. *BMC Bioinform.* **11**, 237 (2010).

640 59. L. J. Zhu, Tiling Arrays, Methods and Protocols. *Methods Mol. Biol.* **1067**, 105–124 (2013).

641 60. F. Ramírez, *et al.*, deepTools2: a next generation web server for deep-sequencing data
642 analysis. *Nucleic Acids Res.* **44**, W160–W165 (2016).

643 61. J. T. Robinson, *et al.*, Integrative genomics viewer. *Nat. Biotechnol.* **29**, 24–26 (2011).

644

645

646 **Figures**

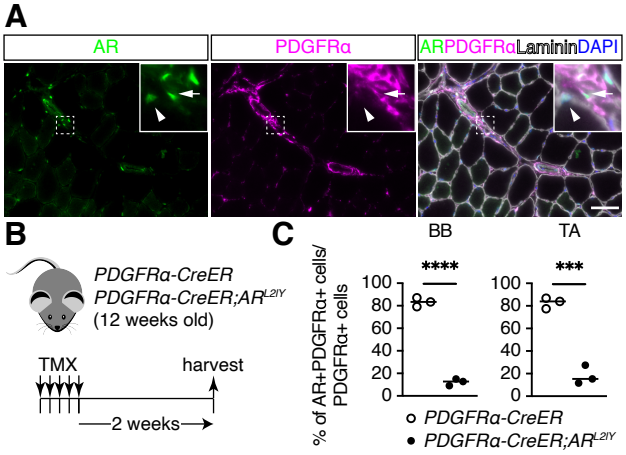

647

648 **Figure 1.** AR ablation in mesenchymal progenitors from *PDGFRα-CreER;AR$^{L2/Y}$* mice. (A)
649 Immunofluorescence staining of AR (left) and PDGFRα (middle) and of both together with
650 laminin and DAPI staining (right) in male TA muscles. Arrows: AR+ and PDGFRα+ cells;
651 arrowheads: AR+ nuclei surrounded by laminin. Scale bar, 50 µm. (B) Experimental design for
652 TMX treatment followed by sample harvest. (C) Quantification of AR+ cells among PDGFRα+
653 cells in the BB (left) and TA (right) muscles of control and mutant mice (n = 3). The two-sample
654 test for equality of proportions: ***$p < 0.001$, ****$p < 0.0001$.

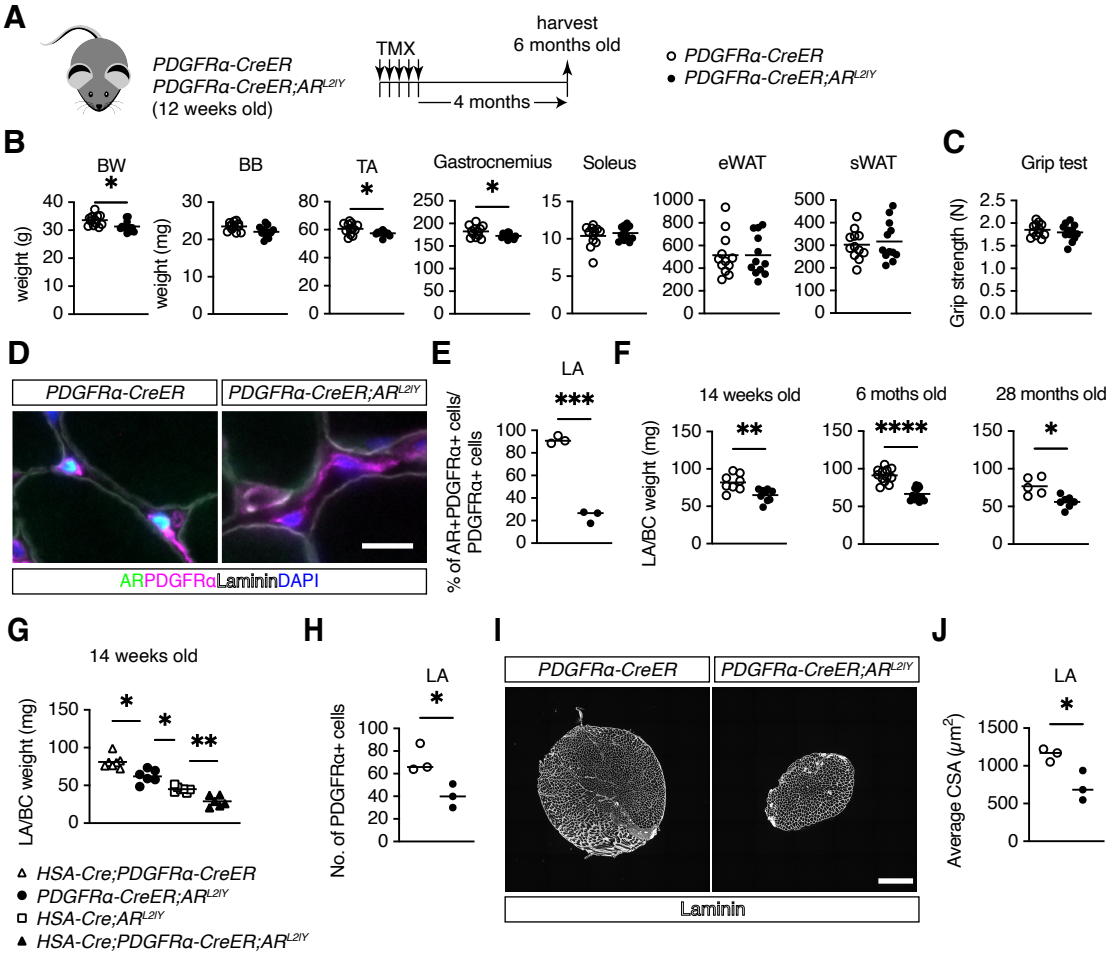

Figure 2. Atrophy of skeletal muscles in mesenchymal progenitor-specific AR-deficient mice. (A) Experimental design for TMX treatment followed by sample harvest in mature adult (6 months old) mice. (B and C) Quantification of body weight (BW), muscle mass, eWAT mass, sWAT mass (B), and grip strength (C) in 6-month-old mice (n = 12). Unpaired t-test with Welch's correction. (D) Immunofluorescence staining of AR, PDGFRα, and laminin with DAPI in LA muscles of control (left) and mutant (right) mice. Scale bar, 10 μm. (E) Quantification of AR+ cells among PDGFRα+ cells in LA muscles of control and mutant mice (n = 3). The two-sample test for equality of proportions. (F) Mass of LA/BC muscles in 14-week-, 6-month-, and 28-month-old mice (n = 5–12). Unpaired t-test with Welch's correction. (G) Mass of LA/BC muscles in single (*HSA-Cre* or *PDGFRα-CreER*) and double Cre mice. Brown-Forsythe and

666 Welch's ANOVA test with Dunnett's T3 multiple comparison test. (H) Quantification of
667 PDGFRα+ cells in LA muscles of control and mutant mice (n = 3). Unpaired t-test with Welch's
668 correction. (I) Immunofluorescence staining of laminin in LA muscles of control (left) and
669 mutant mice (right). Scale bar, 500 µm. (J) Average cross-sectional area (CSA) of myofibers in
670 control and mutant mice (n = 3). Unpaired t-test with Welch's correction: *$p < 0.05$, **$p < 0.01$,
671 ***$p < 0.001$, ****$p < 0.0001$.

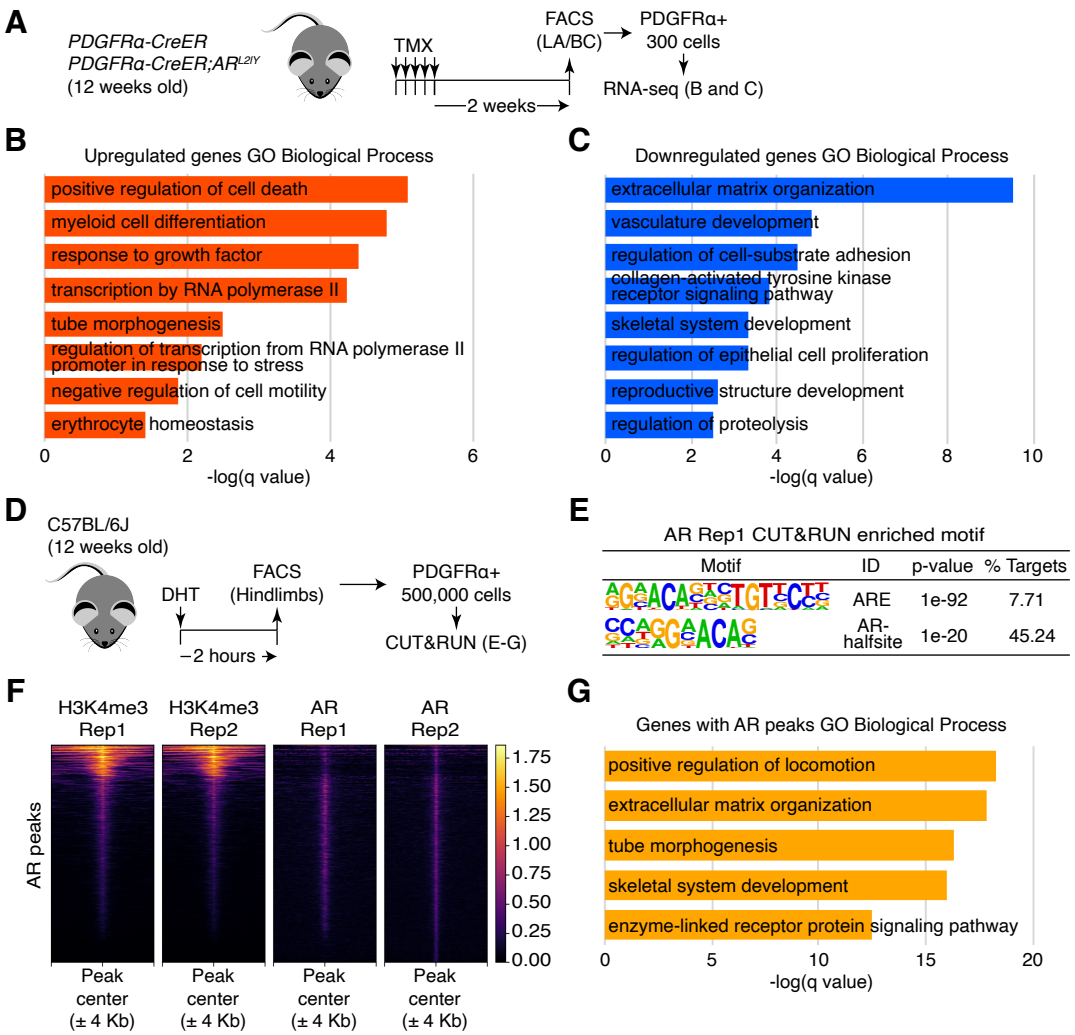

Figure 3. Functional and genomic targets of AR in mesenchymal progenitors of skeletal muscles. (A) Experimental design for TMX treatment followed by fluorescence-activated cell sorting (FACS) and RNA-seq. (B and C) Top Gene Ontology (GO) Biological Process terms associated with the upregulated (B) and downregulated (C) genes in PDGFRα+ cells from mutant mice. (D) Experimental design for DHT treatment followed by FACS and CUT&RUN. (E) Enriched motifs within AR CUT&RUN peaks. (F) Heatmaps of mean H3K4me3 and AR CUT&RUN counts per million (CPM) normalized read coverage around AR CUT&RUN peaks for individual replicates. (G) Top GO Biological Process terms enriched within AR CUT&RUN peak-associated genes.

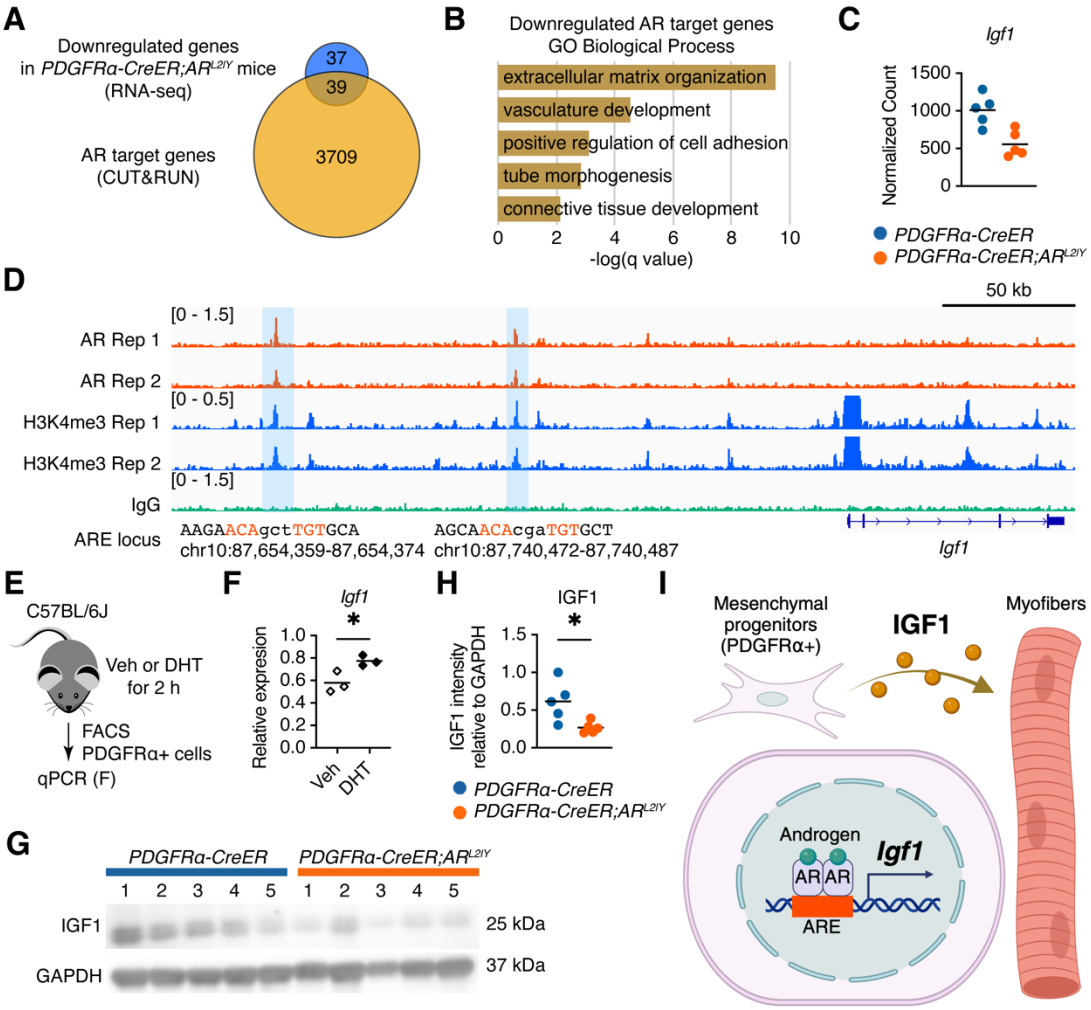

682

683 **Figure 4.** Regulation of Igf1 in mesenchymal progenitors by AR. (A) Overlap of downregulated
684 genes in PDGFRα+ cells from mutant mice and AR CUT&RUN peak-associated genes. (B) Top
685 GO Biological Process terms enriched within overlapped genes. (C) Normalized gene counts for
686 *Igf1* obtained by RNA-seq. (D) AR and H3K4me3 CUT&RUN peaks with androgen response
687 elements (ARE) at *Igf1* locus. The AREs are shown in red. Top left number is the y-axis range in
688 CPM. (E) Experimental design for qPCR after treatment with DHT. (F) qPCR analysis of *Igf1* in
689 PDGFRα+ cells after DHT treatment (n = 3 mice/condition). Unpaired t-test with Welch's
690 correction. (G and H) Western blotting of IGF1 and GAPDH (G) and their quantification (H) in
691 LA muscles from control and mutant mice (n = 5). Unpaired t-test with Welch's correction: *p <

692 0.05. (I) Regulation of IGF1 by AR in mesenchymal progenitors of skeletal muscle. Created with

693 BioRender.com.